*applied sciences*

MDPI

*Article*

# Emergency Dispatch Strategy Considering Spatiotemporal Evolution of Power Grid Failures Under Typhoon Conditions

**Bixing Ren *, Dajiang Wang, Chenggen Wang, Qiang Li, Yingjie Hu and Yongyong Jia**

State Grid Jiangsu Electric Power Company Ltd., Research Institute, Nanjing 211103, China
* Correspondence: renbixing@126.com

**Abstract:** The increasing climate-change-induced tropical cyclone phenomena expose the power grid to significant operation risks by disrupting the normal operation of grid components. This paper considers the failure mechanism with respect to critical grid components and reveals a novel spatiotemporal revolution of grid failures during the passage of typhoons. Based on the spatiotemporal evolution of grid failures, a threshold-based emergency scenario set and the corresponding two-stage robust optimization-based emergency dispatch model are developed. The robust emergency dispatch strategy is obtained using a column-and-constraint generation (C&CG) algorithm. The simulation results show that the proposed robust emergency dispatch strategy can guarantee a considerable degree of robustness under multiple emergency scenarios driven by uncertain typhoon conditions.

**Keywords:** spatiotemporal grid failure; emergency scenario; emergency dispatch



**Citation:** Ren, B.; Wang, D.; Wang, C.; Li, Q.; Hu, Y.; Jia, Y. Emergency Dispatch Strategy Considering Spatiotemporal Evolution of Power Grid Failures Under Typhoon Conditions. *Appl. Sci.* **2024**, *14*, 10368. https://doi.org/10.3390/app142210368

Academic Editor: Andreas Sumper

Received: 12 October 2024
Revised: 31 October 2024
Accepted: 6 November 2024
Published: 11 November 2024



## 1. Introduction

Due to global climate warming, coastal areas within the subtropical monsoon climate zone are increasingly facing safety challenges to the grid operation from tropical cyclones such as typhoons. Unlike sudden natural disasters like earthquakes and fires, tyhoons typically have complete spatiotemporal trajectories, causing damage to power grid equipment and its abnormal characteristics to change over time. Therefore, the distribution of system failures under typhoons exhibits complex spatiotemporal variations. During the spatiotemporal evolution of grid failures, it is imperative to study emergency dispatch strategies that meet the needs of system safety operations, ensuring the security and reliability of grid operation.

The safety risk factors of the modern digital and intelligent power system include new flexible resources such as distributed energy resources and electric vehicles [1,2], extreme weather disasters [3,4], and cyber attacks [5,6]. Among these, extreme weather disasters can cause power grid equipment outages, leading to load shedding and even system splitting issues, which have garnered widespread attention from researchers [7]. Current research primarily focuses on equipment failure analysis [8,9], the identification of critical vulnerable equipment [10], and system risk assessment under extreme weather conditions such as typhoons, extreme heat, and cold waves [11–13]. By analyzing the abnormal mechanisms of extreme weather on equipment, and combining classical equipment aging failure models or data-driven models, the failure probability of the equipment can be determined. The failure probability of a local transmission tower-line system is calculated considering the joint probability distribution of wind speed and direction [14]. A fatigue probability calculation method for wind-turbine towers is developed using the probability density evolution [15]. Based on the solar panel structural performance data, fragility functions for rooftop- and ground-mounted panels are estimated using a Bayesian approach [16]. By generating multiple fault scenarios based on the fault probability characteristics of the equipment and calculating the system operation risk indicators under different fault scenarios, a risk assessment can be achieved. A risk assessment may include a large number of operational

scenarios and their safety risk indicator information, making it difficult for dispatchers to quickly grasp key information. Therefore, by classifying the operational scenarios into risk levels through a severity grading strategy, a risk-level-based early warning method can be obtained [17]. In addition to risk assessment and early warning, researchers are also enhancing the resilience of the power grid to extreme natural disasters through preventive dispatch [18], emergency dispatch [19], and restorative dispatch strategies [20]. Considering the uncertainties of wind power variation, a coordinated method for preventive generation rescheduling and corrective load shedding is proposed to maintain power system transient stability [18]. In [19], a consensus algorithm is developed for energy storage and thermal units to achieve the unit rate of communication [19]. As for restoring the electricity service, a coordinated switch operation and crew dispatch strategy is developed to enhance restorative effectiveness. In addition to treating preventive, emergency, and restorative dispatch separately, some researchers study their coordination [21]. Coordinating different measures can reduce total losses throughout the duration of these events. A novel hierarchical defender–attacker model is employed to coordinate the above dispatch stages, and the robust resilience trapezoid and coordinated strategy is obtained through a nested column-and-constraint generation (C&CG) algorithm [21]. Besides conventional generation, researchers also investigate how to coordinate renewable energy in supporting coordinated multi-stage dispatch [22]. Considering both the short-term emergency and long-term operating limit, a robust preventive–corrective security-constrained optimal power flow is presented under $N - k$ outages [23].

Emergency dispatch during extreme weather events is a crucial element in the three-stage dispatch process. Preventive and restorative dispatches mainly serve as preparatory and backup plans for emergency dispatch, enhancing its effectiveness and preventing the escalation of incidents. Emergency dispatch directly determines whether the system can operate normally under extreme weather conditions. Although researchers have extensively studied emergency dispatch from aspects such as resource types, dispatch objectives, and uncertainties in emergency conditions, few studies have considered the spatiotemporal characteristics of system failures caused by typhoons and their impact on emergency dispatch.

Typhoons have distinct spatiotemporal trajectories, causing power grid equipment to experience varying extreme weather factors at different times, leading to continuously changing equipment failure characteristics. Consequently, the distribution of system failures varies across both temporal and spatial dimensions. The spatiotemporal variation in system failure distribution adds complexity to uncertain emergency conditions, necessitating an accurate depiction of emergency conditions that account for the spatiotemporal changes in anomaly distribution during the passage of typhoon. This will enhance the adaptability and robustness of emergency dispatch plans.

This paper first analyzes the mechanisms by which typhoons cause failures or abnormal states in typical source-grid equipment (wind power plants, poles and conductors) to provide the time-varying abnormal states of wind power and transmission lines, including abnormal wind power output and line fault probability. Based on the spatiotemporal characteristics of grid failures, the fault probability threshold-based emergency scenarios are constructed. A novel robust emergency dispatch strategy is developed using the emergency scenarios under a defender–attacker framework (DAF). Eventually, by recasting the DAF as a two-stage robust optimization model, the robust emergency dispatch of thermal units and energy storage systems is obtained using the C&CG algorithm.

The main contributions of the paper include:

- Considering time-varying abnormal states of typhoon-susceptible grid-source equipment under the spatiotemporal trajectory of typhoons, spatiotemporal characteristics of grid failures are studied. Based on the spatiotemoral grid failures, fault probability threshold-based emergency scenarios during typhoons are developed, thus laying foundations for subsequent emergency dispatch.

- A novel robust emergency dispatch strategy is developed, considering spatiotemporal grid failures during typhoons. Based on the defender–attacker framework, a two-stage robust optimization (TSRO) model is developed, considering the fault probability threshold-based emergency scenarios. The C&CG algorithm is employed to solve the developed TSRO model to obtain the optimal dispatch of various emergency sources such as thermal units and energy storage systems.

The remainder of the paper is organized as follows: Section 2 addresses the spatiotemporal grid failures during typhoons and fault probability-based emergency scenarios; Section 3 studies the robust emergency strategy for the constructed emergency scenarios; Section 4 verfies the developed emergency strategy using the benchmark IEEE 14-bus system. Finally, the last section details the concluding remarks.

## 2. Spatiotemporal Grid Failures and Emergency Scenarios During Typhoons

This section mainly presents the evolution of spatiotemporal grid failures during typhoons. First, considering typical grid-source equipment, including the wind power plants and transmission lines that are susceptible to typhoons, time-varying abnormal states of grid-source equipment and spatiotemporal grid failures are analyzed. Second, novel fault probability threshold-based emergency scenarios are developed considering the spatiotemporal grid failure characteristics.

### *2.1. Abnormal States of Typical Grid-Source Equipment During Typhoons*

#### 2.1.1. Abnormal States of Wind Farm During Typhoons

Usually, once a typhoon enters the 24 h warning zone, meteorological departments continuously update the typhoon's real-time information at 1 h resolutions. For the convenience of analysis, the prediction period of typhoons is set to 24 h, and the sampling time period is set to 1 h. Suppose that the distance between wind farm $i$ at time period $t$ is $r_{i,t}$. The maximal wind speed at time period $t$ is denoted by $v_{\max,t}$. The radius of maximal wind speed is denoted by $R_{\max,t}$. The perceived wind speed of wind farm $i$ can be written by [24]:

$$v_{i,j} = \begin{cases} \frac{r_{i,t}}{R_{\max,t}} v_{\max,t} r_{i,t} \in [0, R_{\max,t}) \\ \frac{R_{\max,t}}{r_{i,t}} v_{\max,t} r_{i,t} \in [R_{\max,t}, \infty) \end{cases} \tag{1}$$

where $r_{i,t}$ is defined by:

$$r_{i,t} = \sqrt{(x_i - x_{o,t})^2 + (y_i - y_{o,t})^2} \tag{2}$$

where $(x_i, y_i)$ represents the fixed coordinate of wind farm $i$; $(x_{o,t}, y_{o,t})$ represents the coordinate of the typhoon center at time period $t$. By substituting the perceived wind speed $v_{i,t}$ into the equivalent wind-turbine power curve function, the abnormal wind power can be expressed by [25]:

$$P_{i,t}^{w} = \begin{cases} \frac{1}{2}\rho v_{i,t}^3 s c_p(\lambda, \beta), v_{in} \le v_{i,t} < v_{rate} \\ P_{rate}^{w}, \quad v_{rate} \le v_{i,t} < v_{out} \\ 0, \quad v_{i,t} \ge v_{out} \end{cases} \tag{3}$$

where $\rho$ represents the air density; $s$ represents the wind-affected area of the rotor blade; $c_p$ represents the power coefficient; $\lambda$ and $\beta$ represent the the tip-speed ratio and pitch angle of the equivalent wind turbine. $v_{in}$, $v_{rate}$, and $v_{out}$ represent the cut-in, rated, and cut-out velocity. $P_{rate}^{w}$ represents the rated wind power. Equations (1)–(3) show that the abnormal wind power $P_{i,t}^{w}$ changes with the movement of the typhoon's position $(x_{o,t}, y_{o,t})$. When the perceived wind speed $v_{i,t}$ is beyond the cut-out speed $v_{out}$, wind farm $i$ will be disconnected from the grid. The wind power $P_{i,t}^{w}$ will fluctuate if the perceived speed $v_{i,t}$ changes drastically with the movement of typhoons. Drastic fluctuations in wind power output can affect the safe operation of the power grid.

2.1.2. Abnormal States of Transmission Line During Typhoons

The elementary components of a transmission line include the conductor and the pole. The pole or tower is a tall vertical structure to support the conductor which transmits electrical energy. Suppose that transmission line $i$ is composed of $M$ poles and $M-1$ interconnected conductors, since the collapse of any pole or conductor will lead to the disconnection of transmission line $i$, the fault probability $Pr_{i,t}(B)$ of line $i$ before time period $t$ can be written by [26]:

$$Pr_{i,t}(B) = \max\left\{ \begin{array}{l} \left[1-\left(1-Pr^{\mathrm{p}}_{1,i,t}(B)\right)\cdots\left(1-Pr^{\mathrm{p}}_{M,i,t}(B)\right)\right] \\ \left[1-\left(1-Pr^{\mathrm{c}}_{1,i,t}(B)\right)\cdots\left(1-Pr^{\mathrm{c}}_{M-1,i,t}(B)\right)\right] \end{array} \right\} \tag{4}$$

where $Pr^{\mathrm{c}}_{k,i,t}(B)$ represents the fault probability of conductor $k$ of line $i$ before time period $t$; $Pr^{\mathrm{p}}_{k,i,t}(B)$ represents the fault probability of pole $k$ of line $i$ before time period $t$.

Equation (25) shows that the fault probability of a transmission line is dependent upon the fault probability of the conductors and poles. The fault probability of the pole is related to the cumulative fatigue damage during typhoons. According to the Palmgren–Miner linear fatigue damage criterion, the cumulative fatigue damage $D$ of a pole can be obtained by summing the fatigue damage over specific time periods. When there is no fatigue damage $D = 0$, the fault probability is zero; when the fatigue damage reaches the threshold value $D = 1$, the fault probability is one and the collapse of the pole is an inevitable event. If the damage value is between zero and one $0 < D < 1$, the pole will have a certain probability of experiencing a collapse. The fatigue damage of a pole during time period $t$ exhibits an exponential relationship with the wind load during that period, where the wind load is proportional to the square of the wind speed. The fatigue damage $D_{k,i,t}$ of conductor $k$ of line $i$ at time period $t$ can be expressed by:

$$D_{k,i,t} = \left\{ \begin{array}{ll} 0, & v_{k,i,t} \in [0, v_{\mathrm{cr}}) \\ ae^{bv^2_{k,i,t}} & v_{k,t} \in [v_{\mathrm{cr}}, v_{\mathrm{m}}) \\ 1, & v_{k,i,t} \in [v_{\mathrm{m}}, \infty) \end{array} \right. \tag{5}$$

where $v_{k,i,t}$ represents the perceived wind speed of conductor $k$ of line $i$ at time period $t$; $a$ and $b$ represent the fatigue coefficient. $v_{\mathrm{cr}}$ represent the threshold wind speed at which the typhoon begins to trigger fatigue in the pole. $v_{\mathrm{m}}$ represents the maximum wind speed corresponding to the one-time damage to the pole, without considering cumulative effects over time. Equation (26) indicates that the one-time damage to the pole is zero when the perceived wind speed is below the threshold wind speed; while the one-time damage to the pole will definitely cause collapse if the perceived wind speed is beyond the maximum.

Equation (26) formulates the one-time damage for a specific time period. In fact, whether a pole collapses depends on the cumulative fatigue damage over multiple time periods. As for the first $q$ time periods, if the cumulative fatigue damage generated in time period $t$ ($t \le q$) from the previous $t-1$ time periods does not lead to a collapse, then the pole will not experience a collapse in the the first $q$ time periods. Therefore, the probability $Pr^{\mathrm{pc}}_{k,i,q}(N)$ of pole $k$ of line $i$ not collapsing in the first $q$ time periods can be expressed as the product of the probabilities of not collapsing from period 1 to $q$.

$$Pr^{\mathrm{pc}}_{k,i,q}(N) = Pr^{\mathrm{p}}_{k,i,1}(N) \cdot Pr^{\mathrm{p}}_{k,i,2}(N) \cdots Pr^{\mathrm{p}}_{k,i,q}(N) \tag{6}$$

where the probability $Pr^{\mathrm{p}}_{k,i,t}(N)$ of pole $k$ of line $i$ not collapsing in the time period $t$ can be expressed by:

$$Pr^{\mathrm{p}}_{k,i,t}(N) = e^{-\frac{D_{k,i,t}}{1-\left(\sum_{s=1}^{t-1} D_{k,i,s}\right)-D_{k,i,t}}}, 1 \le t \le q \tag{7}$$

Equation (7) reflects that the probability of not collapsing in the first $j$ time periods is determined by the combined effect of the cumulative fatigue damage $\sum_{s=1}^{t-1} D_{k,i,s}$ from the

previous $t-1$ time periods and the one-time fatigue damage $D_{k,i,t}$ in the time period $t$. The greater the one-time fatigue damage and cumulative fatigue damage are, the smaller the probability $Pr^{\mathrm{p}}_{k,i,t}(N)$ of the pole not collapsing before time period $t$.

Based on Equations (7) and (27), the probability $Pr^{\mathrm{pc}}_{k,i,q}(N)$ of pole $k$ of line $i$ not collapsing in the first $q$ time periods can be rewritten as:

$$Pr^{\mathrm{pc}}_{k,i,q}(N) = e^{\sum_{t=1}^{q} -\frac{D_{k,i,t}}{1-\left(\sum_{s=1}^{t-1} D_{k,i,s}\right)-D_{k,i,t}}} \tag{8}$$

Equation (8) shows that if the cumulative fatigue damage before period $t-1$ is less than 1 ($\left(\sum_{s=1}^{t-1} D_{k,i,s}\right) < 1$) and the one-time fatigue damage $D_{k,i,t}$ at time period $t$ is zero. The probability of pole $k$ of line $i$ before time period $t$ is only affected by the first $t-1$ time periods. $\left(\sum_{s=1}^{t-1} D_{k,i,s}\right) = 1$ means the cumulative fatigue damage over the first $t$ periods reaches the threshold value 1, the probability of pole $k$ of line $i$ is 1 and the pole will definitely collapse for the first $t$ periods. Based on (8), the probability $\mathrm{Pr}^{\mathrm{pc}}_{k,i,q}(B)$ of pole $k$ of line $i$ collapsing before time period $q$ is:

$$Pr^{\mathrm{p}}_{k,i,q}(B) = 1 - Pr^{\mathrm{pc}}_{k,i,q}(N) \tag{9}$$

The typhoon increases the wind load, which can exceed the conductor's endurance limit, leading to a breakage. In this section, the failure rate $\lambda_{k,i,q}$ of the conductor $k$ of line $i$ at period $q$ is used to calculate the probability of a failure occurring [27]:

$$\lambda_{k,i,q} = \begin{cases} 0, & W_{k,i,q} \in [0, W^{\mathrm{norm}}_{\max}) \\ \frac{(1-\lambda_1)W_{k,i,q}+\lambda_1 W_{\max}-W^{\mathrm{norm}}_{\max}}{W_{\max}-W^{\mathrm{norm}}_{\max}}, & W_{k,i,q} \in [W^{\mathrm{norm}}_{\max}, W_{\max}) \\ 1, & W_{k,i,q} \in [W_{\max}, \infty) \end{cases} \tag{10}$$

where $W_{k,i,q}$ represents the wind pressure endured by conductor $k$ of line $i$ at period $q$; $W^{\mathrm{norm}}_{\max}$ represents the upper limit of normal wind pressure; $W_{\max}$ represents the upper limit of wind pressure; $\lambda_1$ represents the failure rate when the wind pressure is equal to $W^{\mathrm{norm}}_{\max}$.

The probability $R_q$ of no failure before time $q$ can be written as:

$$R_{k,i,q} = R_{k,i,q-1} - \lambda_{k,i,q-1} R_{k,i,q-1} \tag{11}$$

Finally, the fault probability of $Pr^{\mathrm{c}}_{k,i,q}$ of conductor $k$ of line $i$ before time period $q$ is:

$$Pr^{\mathrm{c}}_{k,i,q}(B) = 1 - R_{k,i,q} \tag{12}$$

### *2.2. Evolution of Spatiotemporal Grid Failures and Emergency Scenarios During Typhoons*

Based on (12)–(25) in Section 2.1, we can calculate the fault probability $Pr_{i,j}(B)$ of line $i$ before time period $j$. In consideration of the whole prediction period $T$, the fault probability matrix is expressed by:

$$\mathrm{Pr}(B) = \begin{bmatrix} \mathrm{Pr}_{1,1}(B) & \mathrm{Pr}_{1,2}(B) & \cdots & \mathrm{Pr}_{1,T}(B) \\ \mathrm{Pr}_{2,1}(B) & \mathrm{Pr}_{2,2}(B) & \cdots & \mathrm{Pr}_{2,T}(B) \\ \vdots & \vdots & \cdots & \vdots \\ \mathrm{Pr}_{L,1}(B) & \mathrm{Pr}_{L,2}(B) & \cdots & \mathrm{Pr}_{L,T}(B) \end{bmatrix} \tag{13}$$

Based on (1)–(3), we can obtain the wind power of wind farm $i$ at time period $j$. Figure 1 presents the flowchart of the abnormal spatiotemporal distribution of the power grid during typhoons.

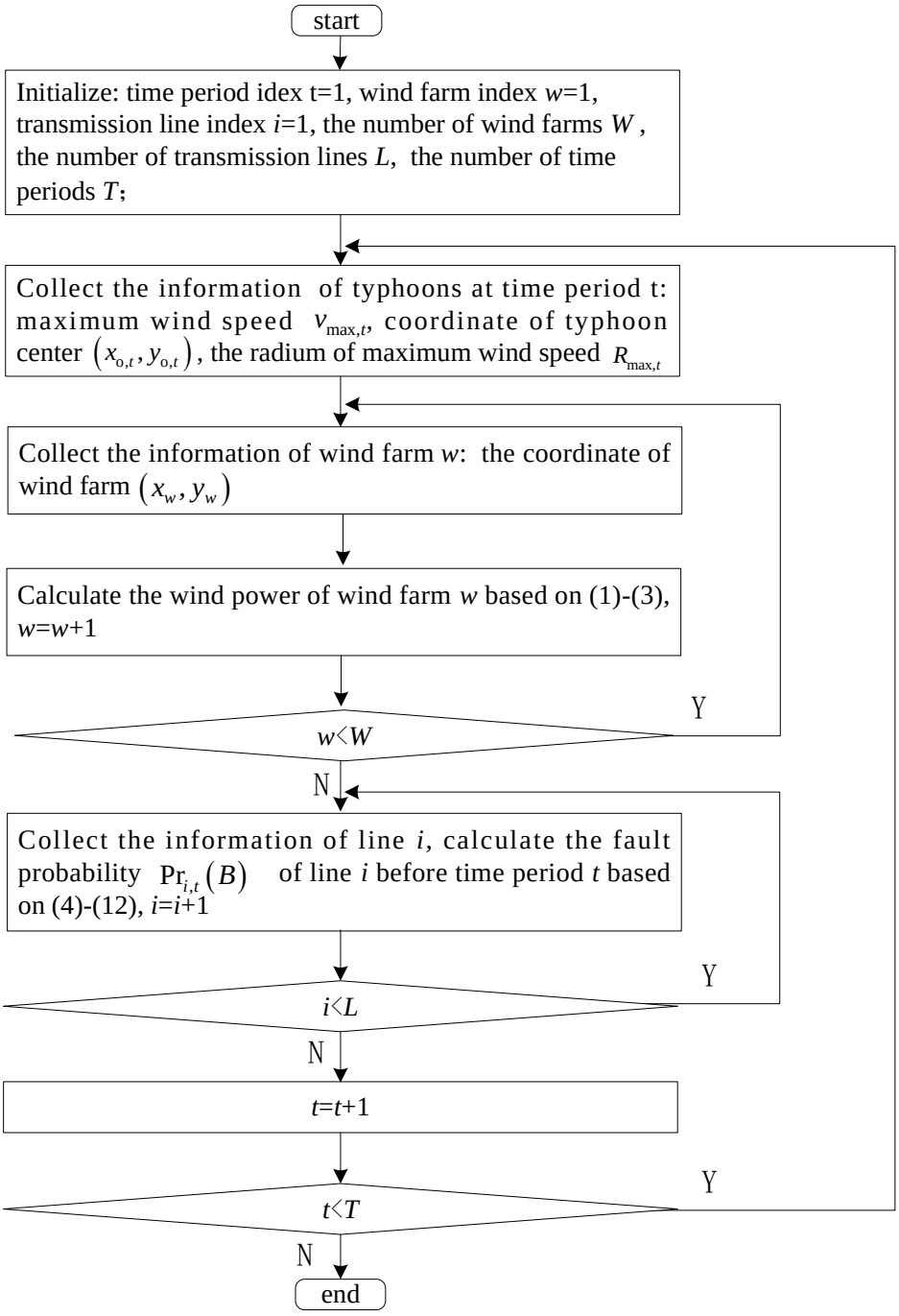


**Figure 1.** Flowchart of the abnormal spatiotemporal distribution of the power grid during typhoons.

The spatiotemporal distribution of transmission lines during typhoons is depicted by a probability matrix. A common method of constructing the emergency scenarios using the probability matrix is to simulate the sufficient numbers of times a line breakage accident occurs. Nevertheless, the large sample size leads to the computational burdens on those small probability events which rarely happen. The probability threshold exists to curb the inclination of the decision maker to overvalue these low-probability threats and to deter the uneconomic over-suppression. In this paper, the probability threshold is used to construct the emergency scenarios. Let $\mu_{i,t} \in \{0, 1\}$ represent the on-off status of line $i$ at period $t$; the on-off status of all affected lines during typhoons can be written as a matrix

form $\boldsymbol{\mu}$. Suppose the probability threshold is $Pr_0$, $t_0$ represents the period in which the fault probability of line $i$ exceeds $Pr_0$ for the first time:

$$t_0 = F_{ij}(Pr_0) \tag{14}$$

where $F_{ij}$ represents the mapping from $Pr_0$ to $t_0$. Then, the sequential on-off statuses of line $ij$ during typhoons are determined as:

$$\mu_{ij,t} = \begin{cases} 1, & if \quad t_0 \notin \mathcal{N}_T \\ 0, & if \quad t_0 \in \mathcal{N}_T \quad and \quad t \geq t_0 \\ 1, & if \quad t_0 \in \mathcal{N}_T \quad and \quad t \leq t_0 \end{cases} \tag{15}$$

where $\mathcal{N}_T$ represents the set of time periods during typhoons. Equation (15) shows that when the fault probability of line $i$ never reaches the threshold $Pr_0$ during typhoons (i.e., $t_0 \notin \mathcal{N}_T$), the status of line $ij$ is always regarded as on-status ($\mu_{ij,t} = 1$). When the fault probability of line $ij$ reaches $Pr_0$ at period $t_0$, the status of line $ij$ after period $t_0$ is regarded as off-status ($\mu_{ij,t} = 0$). In other words, the fault probability is high enough to trigger the breakage; since timely repair is not considered, the off-status lasts for the remaining periods $t \geq t_0$. The status of line $ij$ before period $t_0$ is regarded as on-status ($\mu_{ij,t} = 1$) since the fault probability before period $t_0$ is not big enough to trigger the breakage. In practice, the decision maker can set different $Pr_0$ to reflect the flexibility of their choice of the threshold. Each $Pr_0$ will generate one emergency scenario based on (15). Suppose there are $R$ choices of $Pr_0$, then $R$ emergency scenarios are established.

## 3. Robust Emergency Dispatch Strategy Considering Spatiotemporal Grid Failures During Typhoons

The emergency dispatch resources contain thermal units, energy storage systems (ESSs). By dispatching thermal units and ESSs during typhoons, the negative impact of abnormal wind power and unexpected line outage can be mitigated.

### *3.1. Objective of Emergency Dispatch*

The objective of emergency dispatch is the minimization of the cost of emergency dispatch:

$$\begin{aligned} obj = &\textstyle\sum_t \sum_j \left( a_j \left( P_{j,t}^{\mathrm{g}} \right)^2 + b_j P_{j,t}^{\mathrm{g}}(t) + c_j \right) \\ &+ \textstyle\sum_t \sum_j \left( \lambda_j^{\mathrm{dis}} P_{j,t}^{\mathrm{dis}} + \lambda_j^{\mathrm{cha}} P_{j,t}^{\mathrm{cha}} \right) \end{aligned} \tag{16}$$

where $a_j$, $b_j$, and $c_j$ represent the fuel cost coefficients of thermal unit $j$; $P_{j,t}^{\mathrm{g}}$ represents the output power of thermal unit $j$ at time period $t$; $\lambda_j^{\mathrm{cha}}$ and $\lambda_j^{\mathrm{dis}}$ represent the charge and discharge cost coefficient of ESS $j$; $P_{j,t}^{\mathrm{cha}}$ and $P_{j,t}^{\mathrm{dis}}$ represent the charge and discharge power of ESS $j$ at period $t$, respectively.

### *3.2. Operational Constraints of Emergency Dispatch*

The output power $P_{j,t}^{\mathrm{g}}$ of thermal unit $j$ at time period $t$ should satisfy the upper and lower output limit constraints:

$$P_j^{\mathrm{g,min}} \leq P_{j,t}^{\mathrm{g}} \leq P_j^{\mathrm{g,max}} \tag{17}$$

where $P_j^{\mathrm{g,min}}$ and $P_j^{\mathrm{g,max}}$ represent the lower and upper power limits of thermal unit $j$.

The ramping limit of thermal units is expressed by:

$$P_j^{\mathrm{rd}} \leq P_{j,t}^{g} - P_{j,t}^{g} \leq P_j^{\mathrm{ru}} \tag{18}$$

where $P_j^{\mathrm{rd}}$ and $P_j^{\mathrm{ru}}$ represent the ramp-down and ramp-up limits of unit $j$.

The discharge and charge power limits of ESS $j$ satisfy:

$$0 \le P_{j,t}^{\mathrm{dis}} \le \beta_{j,t}^{\mathrm{dis}} P_j^{\mathrm{dis,max}} \tag{19}$$

$$0 \le P_{j,t}^{\mathrm{cha}} \le \beta_{j,t}^{\mathrm{cha}} P_j^{\mathrm{cha,max}} \tag{20}$$

where $P_{j,t}^{\mathrm{dis}}$ and $P_{j,t}^{\mathrm{cha}}$ represent the discharge and charge power of ESS $j$ at time period $t$; $\beta_{j,t}^{\mathrm{dis}}$ and $\beta_{j,t}^{\mathrm{cha}}$ ($\beta_{j,t}^{\mathrm{dis}}, \beta_{j,t}^{\mathrm{cha}} \in \{0,1\}$) represent the discharge and charge status of ESS $j$ at time period $t$; $P_j^{\mathrm{dis,max}}$ and $P_j^{\mathrm{cha,max}}$ represent the maximum discharge and charge power of ESS $j$.

An ESS cannot be in both discharging and charging states simultaneously:

$$\beta_{j,t}^{\mathrm{dis}} + \beta_{j,t}^{\mathrm{cha}} = 1 \tag{21}$$

The relation between the stored energy and the discharge or charge power of an ESS is:

$$E_{j,t} = E_{j,t-1} - P_{j,t}^{\mathrm{dis}} \Big/ \eta_j^{\mathrm{dis}} + P_{j,t}^{\mathrm{cha}} \eta_j^{\mathrm{cha}} \tag{22}$$

where $E_{j,t}$ represent the stored energy of ESS $j$ at period $t$; $\eta_j^{\mathrm{cha}}$ and $\eta_j^{\mathrm{dis}}$ represent the charge and discharge efficiency coefficient of ESS $j$.

The stored energy $E_{j,t}$ of ESS $j$ at period $t$ should satisfy:

$$E_{j,\min} \le E_{j,t} \le E_{j,\max} \tag{23}$$

where $E_{j,\min}$ and $E_{j,\max}$ represent the minimum and maximum energy of ESS $j$.

The nodal power balance of node $j$ is written by:

$$\begin{aligned} &\alpha_j^{\mathrm{g}} P_{j,t}^{\mathrm{g}} + \alpha_j^{\mathrm{e}} \left( P_{j,t}^{\mathrm{dis}} - P_{j,t}^{\mathrm{cha}} \right) + \alpha_j^{\mathrm{w}} P_{j,t}^{\mathrm{w}} \\ &-\alpha_j^{\mathrm{d}} P_{j,t}^{\mathrm{d}} = \sum_{k \in \Omega_t} P_{jk,t} - \sum_{i \in \Omega_f} P_{ij,t} \end{aligned} \tag{24}$$

where $\alpha_j^{\mathrm{g}}$, $\alpha_j^{\mathrm{e}}$, $\alpha_j^{\mathrm{w}}$, $\alpha_j^{\mathrm{d}}$ represent the identifier, indicating whether node $j$ is installed with a thermal unit, ESS, wind farm, or load. $\alpha_j^{\mathrm{g,e,w,d}} = 1$ indicate whether node $j$ is installed with a thermal unit, ESS, wind farm, or load; $\alpha_j^{\mathrm{g,e,w,d}} = 0$ indicates that node $j$ is not installed with a thermal unit, ESS, wind farm, or load. $\Omega_t$ represents the set of to-nodes interconnected with node $j$; $\Omega_f$ represents the set of from-nodes interconnected with node $j$; $P_{jk,t}$ represent the power flow from node $j$ to node $k$ at time period $t$; $P_{ij,t}$ represent the power flow from node $i$ to node $j$ at time period $t$.

The power flow equation describing the relationship between the transmitted power and the phase angles at both ends of the line can be expressed by:

$$P_{ij,t} = B_{ij}\left(\theta_{i,t} - \theta_{j,t}\right) \tag{25}$$

where $P_{ij,t}$ represents the transmitted power from node $i$ to node $j$ at time period $t$; $B_{ij}$ denotes the susceptance of the line between node $i$ and $j$; $\theta_{i,t}$ and $\theta_{j,t}$ represent the phase angle of node $i$ and $j$ at time period $t$.

If the line between node $i$ and $j$ is disconnected due to the fatigue damage caused by typhoons, Equation (25) does not hold and $P_{ij,t}$ can be any value; while Equation (25) holds if the line between node $i$ and $j$ is connected. Hence, the power flow can be rewritten as:

$$B_{ij}\left(\theta_{i,t} - \theta_{j,t}\right) + P_{ij,t} \le \left(1 - \mu_{ij,t}\right) M \tag{26}$$

$$B_{ij}\left(\theta_{i,t} - \theta_{j,t}\right) + P_{ij,t} \ge \left(\mu_{ij,t} - 1\right) M \tag{27}$$

where $\mu_{ij,t} \in \{0,1\}$ represents the on–off status of the line between node $i$ and $j$ at time period $t$. $M$ is a large positive number. When the line between node $i$ and $j$ at time period $t$ is connected (i.e., $\mu_{ij,t} = 1$), Equations (26) and (27) are transformed into (25). When the line between node $i$ and $j$ at time period $t$ is connected (i.e., $\mu_{ij,t} = 0$), there is no obvious relation between $P_{ij,t}$ and $B_{ij}\left(\theta_{i,t} - \theta_{j,t}\right)$, and $P_{ij,t}$ can be any value between $-M$ and $M$.

### *3.3. Robust Emergency Dispatch Strategy During Typhoons*

Based on Section 3.1, the two-stage robust optimization (TSRO) model under the attacker-defender framework is recast as:

$$\begin{aligned} &\min_{\boldsymbol{y}\in\Omega_y} \max_{\boldsymbol{\mu}\in\Omega_\mu} \min_{\boldsymbol{x}} obj \\ &\text{s.t.} \quad \boldsymbol{G}_1\boldsymbol{x} + \boldsymbol{G}_2\boldsymbol{y} + \boldsymbol{G}_3\boldsymbol{\mu} + \boldsymbol{G}_4\boldsymbol{h} \le 0 \end{aligned} \tag{28}$$

where the binary ESS status $\boldsymbol{y} = \left[\beta_{j,t}^{\text{dis}}, \beta_{j,t}^{\text{cha}}\right]$ are the first-stage decision variables; while $\boldsymbol{x} = \left[P_{j,t}^{\text{dis}}, P_{j,t}^{\text{dis}}, P_{j,t}^{\text{g}}\right]$ are the second-stage decision variables. $\boldsymbol{\mu} \in \Omega_\mu$ represents the set of $R$ emergency scenarios constructed from Section 2.2. The constraint represents (17)–(27). $\boldsymbol{G}_1$, $\boldsymbol{G}_2$, $\boldsymbol{G}_3$, and $\boldsymbol{G}_4$ represent the corresponding matrices; $\boldsymbol{h} = \left[E_{j,t}, P_{ij,t}, \theta_{ij,t}\right]$ are the intermediate variables.

As can be seen, the max–min operator in (28) makes the second stage a defender–attacker model. The attacker (typhoon) attempts to maximize the emergency dispatch cost by applying the severest emergency scenario; while the defender (dispatcher) attempts to minimize the dispatch cost. The max operator means that the dispatch cost under the severest emergency scenario is larger than that under other emergency scenarios. Therefore, Equation (28) can be reformulated as the following:

$$\begin{aligned} &\min_{\boldsymbol{y}\in\Omega_y} \eta \\ &s.t. \quad \eta \ge obj_r, \quad r = 1, \cdots, R \\ &\quad \boldsymbol{G}_1\boldsymbol{x}_r + \boldsymbol{G}_2\boldsymbol{y} + \boldsymbol{G}_3\boldsymbol{\mu}_r + \boldsymbol{G}_4\boldsymbol{h}_r \le 0, \quad r = 1, \cdots, R \end{aligned} \tag{29}$$

where $\boldsymbol{x}_r$ represent the optimal solutions of the second-stage decision variables corresponding to emergency scenario $r$. $\boldsymbol{\mu}_r$ represent the on–off line statuses under emergency scenario $r$. $\boldsymbol{h}_r$ represent the optimal solutions of the second-stage intermediate variables corresponding to emergency scenario $r$.

As a result, solving (28) reduces to solve an equivalent (29). Rather than enumerating all the emergency scenarios and solving (29), a column-and-constraint generation (C&CG) procedure is implemented in a master–subproblem framework. The procedure is as follows:

1. Set the lower boundary to the negative infinity $LB = -\infty$ and the upper boundary to the positive infinity $UB = \infty$; set the counter to zero $k = 0$; initialize the set of counter $\boldsymbol{O} = \emptyset$; initialize the error threshold $\epsilon$.
2. Solve the master problem

$$\begin{aligned} &\min_{\boldsymbol{y},\eta} \eta \\ &s.t. \quad \eta \ge obj_r, \qquad \forall r \in \boldsymbol{O} \\ &\quad \boldsymbol{G}_1\boldsymbol{x}_r + \boldsymbol{G}_2\boldsymbol{y} + \boldsymbol{G}_3\boldsymbol{\mu}_r^* + \boldsymbol{G}_4\boldsymbol{h}_r \le 0, \forall r \le k \\ &\quad \boldsymbol{y} \in \Omega_y \end{aligned} \tag{30}$$

   Derive the optimal solutions $(\boldsymbol{y}_{k+1}^*, \eta_{k+1}^*, \boldsymbol{x}_1^*, \cdots, \boldsymbol{x}_r^*)$ and update the lower boundary $LB = \eta_{k+1}^*$
3. Solve the sub-problem $\mathcal{Q}(\boldsymbol{y}_{k+1}) = \left\{ \max_{\boldsymbol{\mu}\in\Omega_\mu} \min_{\boldsymbol{x}} obj : \boldsymbol{G}_1\boldsymbol{x} + \boldsymbol{G}_2\boldsymbol{y} + \boldsymbol{G}_3\boldsymbol{\mu} + \boldsymbol{G}_4\boldsymbol{h} \le 0 \right\}$ and update the upper boundary $UB = \mathcal{Q}(\boldsymbol{y}_{k+1}^*)$.
4. If $UB - LB \le \epsilon$, return $\boldsymbol{y}_{k+1}^*, \boldsymbol{x}_k^*$, and terminate. Otherwise,

– (a) if $\mathcal{Q}(\boldsymbol{y}^*_{k+1}) < \infty$, create variables $\boldsymbol{x}_{k+1}$ and $\boldsymbol{h}_{k+1}$ in the $k+1$-th iteration and add the optimality cuts

$$\eta \geq obj_{k+1} \tag{31}$$

$$\boldsymbol{G}_1\boldsymbol{x}_{k+1} + \boldsymbol{G}_2\boldsymbol{y} + \boldsymbol{G}_3\boldsymbol{\mu}^*_{k+1} + \boldsymbol{G}_4\boldsymbol{h}_{k+1} \leq 0 \tag{32}$$

to the master problem, where $\boldsymbol{\mu}^*_{k+1}$ is the optimal emergency scenario by solving $\mathcal{Q}(\boldsymbol{y}_{k+1})$. Update $k = k+1$, $\boldsymbol{Q} = \boldsymbol{Q} \cup k+1$, go to step 2.

– (b) if $\mathcal{Q}(\boldsymbol{y}^*_{k+1}) = \infty$, create variables $\boldsymbol{x}_{k+1}$ and $\boldsymbol{h}_{k+1}$ in the $k+1$-th iteration and add the feasibility cuts

$$\boldsymbol{G}_1\boldsymbol{x}_{k+1} + \boldsymbol{G}_2\boldsymbol{y} + \boldsymbol{G}_3\boldsymbol{\mu}^*_{k+1} + \boldsymbol{G}_4\boldsymbol{h}_{k+1} \leq 0 \tag{33}$$

to the master problem, where $\boldsymbol{\mu}^*_{k+1}$ is the optimal emergency scenario by solving $\mathcal{Q}(\boldsymbol{y}_{k+1})$. Update $k = k+1$, go to step 2.

## 4. Case Studies

This section presents the case studies using the benchmark IEEE-14 bus system under Typhoon Maria. The trajectory of Typhoon Maria during the 24 h periods is shown in Figure 2. Based on the proposed robust emergency dispatch strategy in (1)–(33), the M-file-based program is established using Python 3.9 and solved by Pyomo 6.8.0. All case studies in this paper are conducted on a laptop with an 8-core Intel i7-9750H processor and 16 GB RAM (Intel Corporation, Santa Clara, CA, USA). The excution time is 18.54 s. The timeliness for the application in real-life systems is also affected by factors such as signal transmission time, and delayed response time.

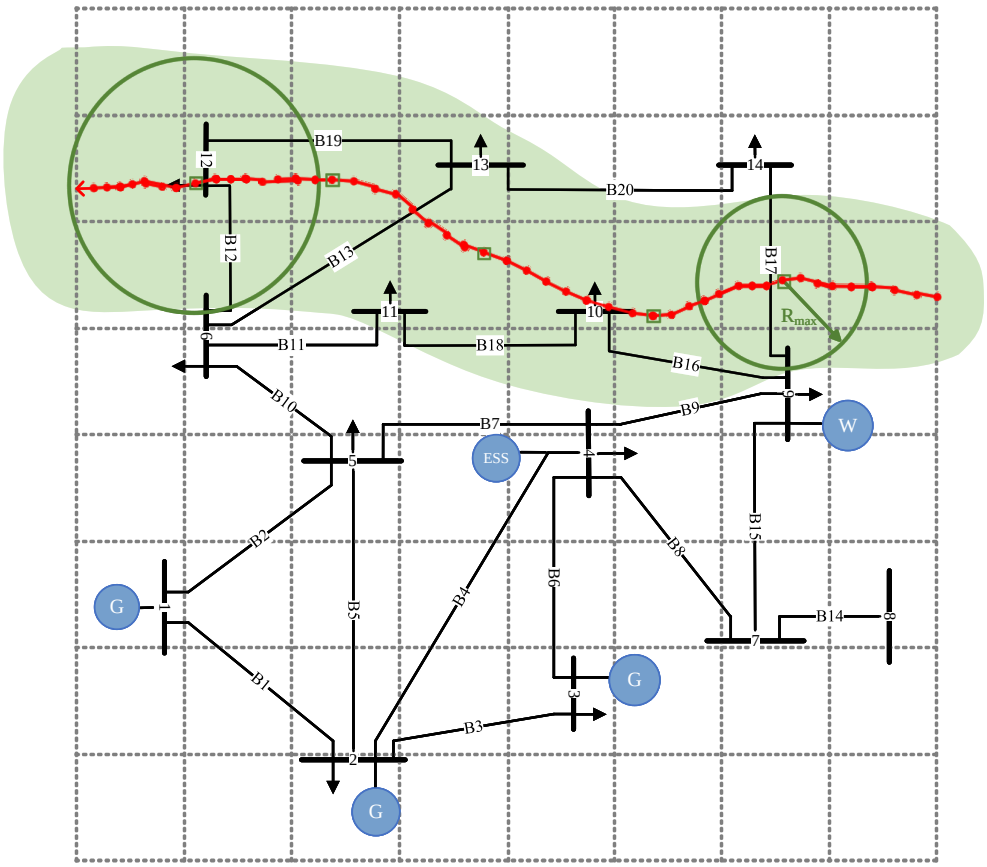


**Figure 2.** Schematic diagram of IEEE-14 bus system under Typhoon Maria over 24 h (green area represents the region swept by the typhoon).

### 4.1. Parameter Setting

The typical parameters of Typhoon Maria are given in Table 1.

**Table 1.** Typical parameters of Typhoon Maria over 24 h periods.

| Parameter | 1 h | 2 h | 3 h | 4 h |
|---|---|---|---|---|
| $v_{max,i}$ | 48 m/s | 50 m/s | 50 m/s | 48 m/s |
| $R_{max,i}$ | 25.1 m | 24.5 m | 30.2 m | 27.6 m |
| $(x_{o,i}, y_{o,i})$ | (123.9 E, 25.4 N) | (123.6 E, 25.5 N) | (123.4 E, 25.6 N) | (123.1 E, 25.8 N) |
| Parameter | 5 h | 6 h | 7 h | 8 h |
| $v_{max,i}$ | 48 m/s | 48 m/s | 48 m/s | 48 m/s |
| $R_{max,i}$ | 28.4 m | 28.4 m | 26.2 m | 23.2 m |
| $(x_{o,i}, y_{o,i})$ | (122.7 E, 25.9 N) | (122.3 E, 26.1 N) | (121.9 E, 26.3 N) | (121.4 E, 26.3 N) |
| Parameter | 9 h | 10 h | 11 h | 12 h |
| $v_{max,i}$ | 45 m/s | 45 m/s | 45 m/s | 43 m/s |
| $R_{max,i}$ | 25.8 m | 22.4 m | 27.3 m | 32.8 m |
| $(x_{o,i}, y_{o,i})$ | (121.0 E, 26.3 N) | (120.8 E, 26.3 N) | (120.6 E, 26.4 N) | (120.3 E, 26.4 N) |
| Parameter | 13 h | 14 h | 15 h | 16 h |
| $v_{max,i}$ | 43 m/s | 43 m/s | 43 m/s | 40 m/s |
| $R_{max,i}$ | 32.5 m | 32.8 m | 39.4 m | 39.9 m |
| $(x_{o,i}, y_{o,i})$ | (119.9 E, 26.4 N) | (119.5 E, 26.3 N) | (119.1 E, 26.2 N) | (118.9 E, 26.3 N) |
| Parameter | 17 h | 18 h | 19 h | 20 h |
| $v_{max,i}$ | 40 m/s | 40 m/s | 40 m/s | 40 m/s |
| $R_{max,i}$ | 35.9 m | 39.9 m | 39.4 m | 37.5 m |
| $(x_{o,i}, y_{o,i})$ | (118.7 E, 26.4 N) | (118.4 E, 26.5 N) | (118.1 E, 26.7 N) | (117.8 E, 26.9 N) |
| Parameter | 21 h | 22 h | 23 h | 24 h |
| $v_{max,i}$ | 40 m/s | 40 m/s | 40 m/s | 38 m/s |
| $R_{max,i}$ | 41.1 m | 43.7 m | 45.7 m | 42.8 m |
| $(x_{o,i}, y_{o,i})$ | (117.6 E, 27.0 N) | (117.4 E, 27.1 N) | (117.2 E, 27.1 N) | (117.0 E, 27.1 N) |

The thermal units participating in emergency dispatch are installed as nodes 1, 2, and 3. Table 2 provides the typical parameters of thermal units.

**Table 2.** Typical parameters of thermal units participating in emergency dispatch.

| ID | $P_j^{g,min}$ | $P_j^{g,max}$ | $a_j, b_j, c_j$ | $P_j^{rd}, p_j^{ru}$ |
|---|---|---|---|---|
| 1 | 3 p.u. | 0.25 p.u. | 0.043, 20, 0 \$/p.u. | −0.35, 0.35 p.u./h |
| 2 | 1.5 p.u. | 0.15 p.u. | 0.25, 20, 0 \$/p.u. | −0.35, 0.35 p.u./h |
| 3 | 1 p.u. | 0.1 p.u. | 0.01, 40, 0 \$/p.u. | −0.35, 0.35 p.u./h |

The ESS participating in emergency dispatch is labeled as node 4. The typical parameters are given in Table 3

**Table 3.** Typical parameters of ESS participating in emergency dispatch.

| $P_j^{dis,max(cha,max)}$ | $E_{j,min}$ | $E_{j,max}$ | $\eta_j^{dis(cha)}$ | $\lambda_j^{cha}$ | $\lambda_j^{dis}$ |
|---|---|---|---|---|---|
| 0.2 p.u. | 0.54 p.u. | 0.06 p.u. | 0.9 | 20\$/p.u. | 22\$/p.u. |

The typical parameters of identifying abnormal states of wind power and transmission lines are listed in Table 4.

**Table 4.** Typical parameters of identifying abnormal states in emergency dispatch.

| $v_{out}$ | $v_{cr}$ | $v_m$ | $W_{\max}^{\text{norm}}$ | $W_{\max}$ |
|---|---|---|---|---|
| 25 m/s | 20 m/s | 53 m/s | 0.7 kN/m$^2$ | 2.1 kN/m$^2$ |

The system data of IEEE-14 bus system is presented in Table 5.

**Table 5.** Line data of IEEE-14 bus system.

| Line ID | From Bus | To Bus | Reactance | MVA Rating |
|---|---|---|---|---|
| 1 | 1 | 2 | 0.06 p.u. | 120 MVA |
| 2 | 1 | 5 | 0.22 p.u. | 65 MVA |
| 3 | 2 | 3 | 0.20 p.u. | 36 MVA |
| 4 | 2 | 4 | 0.18 p.u. | 65 MVA |
| 5 | 2 | 5 | 0.17 p.u. | 50 MVA |
| 6 | 3 | 4 | 0.17 p.u. | 65 MVA |
| 7 | 4 | 5 | 0.04 p.u. | 45 MVA |
| 8 | 4 | 7 | 0.21 p.u. | 55 MVA |
| 9 | 4 | 9 | 0.56 p.u. | 32 MVA |
| 10 | 5 | 6 | 0.25 p.u. | 45 MVA |
| 11 | 6 | 11 | 0.20 p.u. | 18 MVA |
| 12 | 6 | 12 | 0.26 p.u. | 32 MVA |
| 13 | 6 | 13 | 0.13 p.u. | 32 MVA |
| 14 | 7 | 8 | 0.18 p.u. | 32 MVA |
| 15 | 7 | 9 | 0.11 p.u. | 32 MVA |
| 16 | 9 | 10 | 0.08 p.u. | 32 MVA |
| 17 | 9 | 14 | 0.27 p.u. | 32 MVA |
| 18 | 10 | 11 | 0.19 p.u. | 12 MVA |
| 19 | 12 | 13 | 0.20 p.u. | 12 MVA |
| 20 | 13 | 14 | 0.35 p.u. | 12 MVA |

In the planning and management of power systems or other critical infrastructures, since even disaster events with very low probabilities should be taken seriously, large values should not be set for the threshold $Pr_0$, to contain more "low-probability" emergency scenarios for emergency dispatch. In this paper, the range of $Pr_0$ is set $(0.1, 0.5)$.

### *4.2. Evolution of Spatiotemporal Grid Failures of IEEE 14-Bus System During Typhoon Maria*

Based on the spatiotemporal parameters of Typhoon Maria in Section 4.2, the evolution of spatiotemporal grid failures of IEEE 14-bus system is obtained by calculating the fault probability matrix $Pr(B)$ in (13). $Pr(B)$ is calculated and then visualized as a heatmap in Figure 3.

As shown in Figure 3, the failure probability of each line increases over time. Lines 9, 16, and 17 have significant high-failure probabilities, because they are the first lines that suffer from the typhoon during its passage. Among them, Line 17 has the highest fault probability (0.78) since it is closest to the typhoon and has the greatest cumulative fatigue damage. Additionally, as the wind weakens, the cumulative damage caused by Typhoon Maria to subsequent lines decreases, and the fault probability of these lines less affected by Typhoon Maria remain at a low level (less than 0.1). The range $(0.1, 0.7)$ of $Pr_0$ is partitioned into seven equal parts with the interval 0.1, i.e., $Pr_0 = \{0.1, 0.2, 0.3, \cdots, 0.7\}$. Then, based on (15), seven on–off line status matrices are calculated to construct the set $\Omega_\mu$ of 10 emergency scenarios.

Figure 4 shows the on–off statuses of 20 lines over 24 h of Typhoon Maria's passage under different $Pr_0$. As for each heatmap, the horizontal axis represents the period number; and the vertical axis represents the line number. $state(i, j) = 0$ indicates that line $j$ at period $i$ is disconnected, while $state(i, j) = 1$ indicates that line $j$ at period $i$ is connected. Figure 4a shows that small $Pr_0 = 0.1$ leads to more line failures indicated by 0 in the heatmap

compared with other $Pr_0$ values. When the decision maker does not hold a conservative stance and only pays attention to those high-probability events by setting the threshold $Pr_0 = 0.7$, only lines 9 and 17, which are heavily affected by Typhoon Maria, experience the outage accidents.

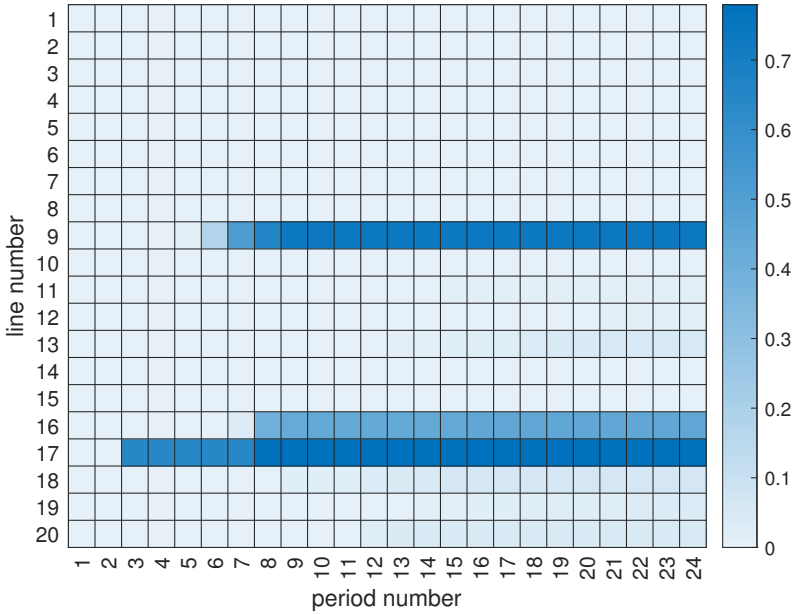


**Figure 3.** Fault probability of lines during Typhoon Maria.

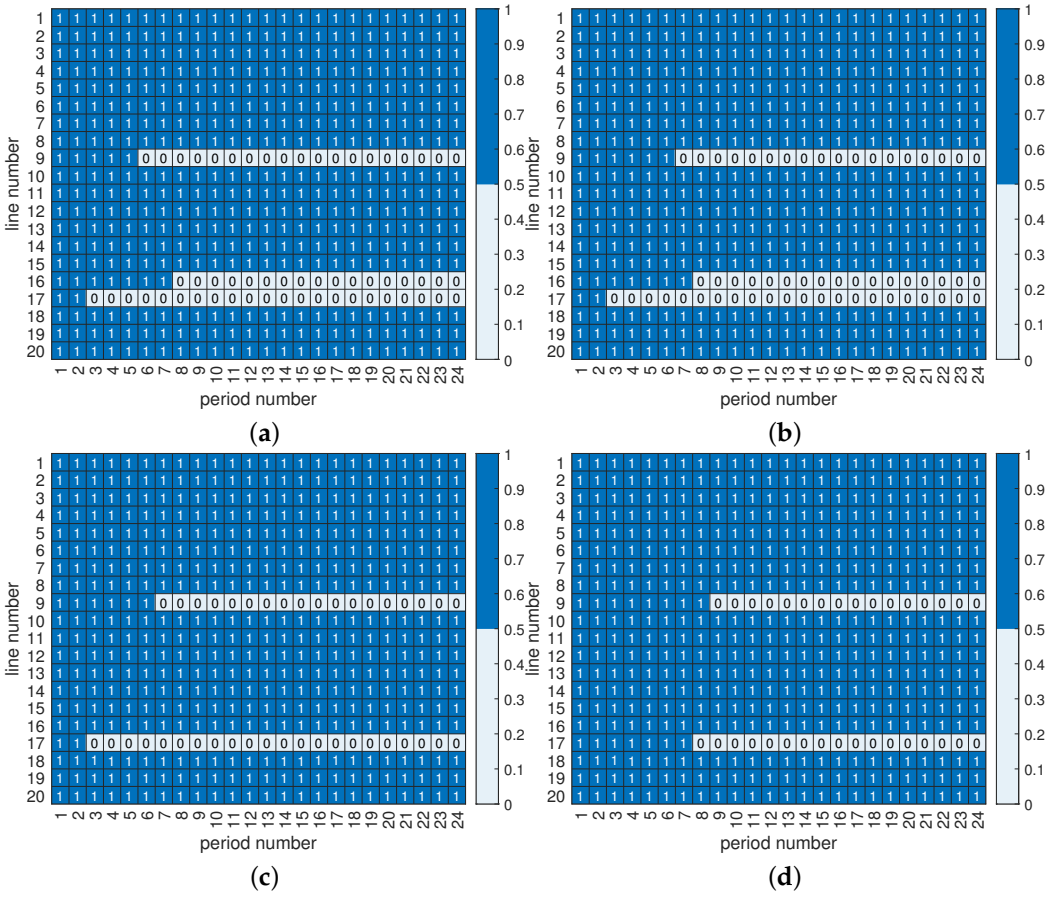


**Figure 4.** Emergency scenarios under (**a**) scenario 1 $Pr_0 = 0.1$ (**b**) scenario 2 $Pr_0 = 0.3$ (**c**) scenario 3 $Pr_0 = 0.5$ (**d**) scenario 4 $Pr_0 = 0.7$.

### *4.3. Coordinated Emergency Dispatch of Thermal Units and ESSs*

Based on the generated emergency scenarios in Section 4.2, the emergency dispatch model in (28) is developed and solved by the procedures in Section 3.3. Figure 5 shows the time-series output power of thermal units (i.e., G1, G2, and G3), ESS during Typhoon Maria. Since G1 has the lowest cost among thermal units and the ESS, G1 bears the main responsibility of power generation. Due to the ramping limits, the three thermal units cannot immediately satisfy the demand from 1–2 h, and the ESS bears the remainder that cannot be covered by thermal units. After 2 h, the expensive ESS withdraws, since the power of thermal units has increased high enough to cover the load.

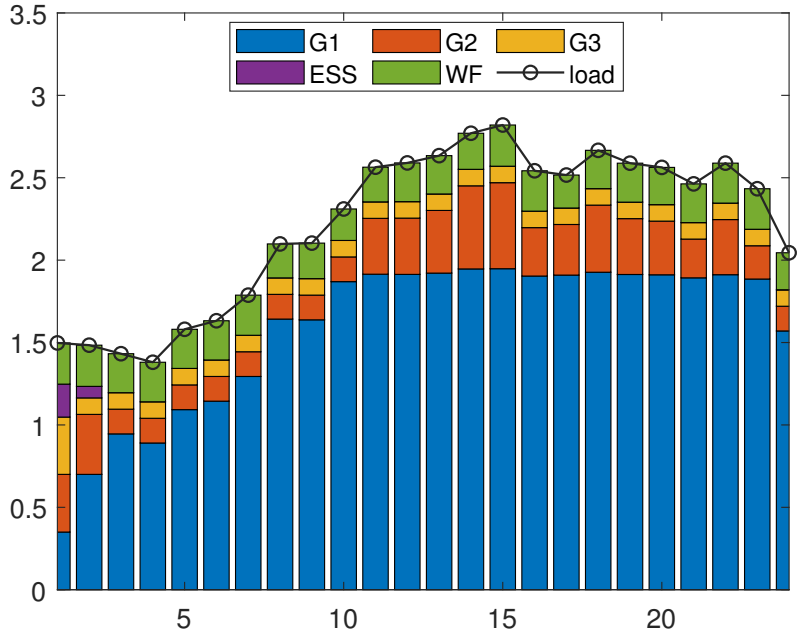


**Figure 5.** Sequential output power of emergency dispatch resources.

To evaluate the robustness of the proposed strategy, the non-robust strategy is generated singly for the emergency scenario 1 in Figure 4a. Then the non-robust strategy is tested on the emergency scenario 2–4 in Figure 4b–d. The unexpected load and wind power curtailment cost is defined to evaluate the robustness. The calculation of the unexpected load and wind power curtailment cost is defined as an optimization problem. The objective is to minimize the unexpected load and wind power curtailment cost.

$$\min \sum_t \sum_j \lambda_j^d \Delta P_{j,t}^d + \sum_t \sum_j \lambda_j^w \Delta P_{j,t}^w \tag{34}$$

Since the component-level regulation characteristic constraints (17)–(23) of respective emergency dispatch resources always hold for the given optimal $\{P_{j,t}^{g*}, P_{j,t}^{dis*}, P_{j,t}^{cha*}, E_{j,t}^*\}$ using either the non-robust or the robust strategy, only the system-level power flow-related constraints are considered. The revised nodal power balance of node $j$ is written by:

$$\begin{aligned} &\alpha_j^g P_{j,t}^{g*} + \alpha_j^e \left(P_{j,t}^{dis*} - P_{j,t}^{cha*}\right) + \alpha_j^w (P_{j,t}^w - \Delta P_{j,t}^w) \\ &-\alpha_j^d (P_{j,t}^d - \Delta P_{j,t}^d) = \sum_{k \in \Omega_t} P_{jk,t} - \sum_{i \in \Omega_f} P_{ij,t} \end{aligned} \tag{35}$$

The revised power flow equations are:

$$B_{ij}(\theta_{i,t} - \theta_{j,t}) + P_{ij,t} \le \left(1 - \mu_{ij,t}^{\epsilon}\right) M \tag{36}$$

$$B_{ij}\left(\theta_{i,t}-\theta_{j,t}\right)+P_{ij,t}\geq\left(\mu_{ij,t}^{\epsilon}-1\right)M \tag{37}$$

where $\mu_{ij,t}^{\epsilon}$ represent the on–off status of the line between node $i$ and $j$ at time period $t$ under emergency scenario $\epsilon$. The definition of other variables or parameters are the same as those in (36) and (37). By running the non-robust and robust strategy using (35)–(37) under four emergency scenarios in Figure 4, the unexpected load and wind power curtailment costs are given in Table 6. Due to the similarity between emergency scenario 1 and 2, the non-robust strategy for emergency scenario 1 can be applied to emergency scenario 2 without incurring load and wind power curtailment costs. However, when applying non-robust strategy to emergency scenario 3 and 4, there will be unexpected load and wind power curtailment costs (2.31e5$). In contrast, the proposed robust strategy can guarantee no more curtailment costs under all four emergency scenarios.

**Table 6.** Load and wind power curtailment costs under different emergency scenarios.

| Strategy | Scenario 1 | Scenario 2 | Scenario 3 | Scenario 4 |
|---|---|---|---|---|
| non-robust strategy | 0$ | 0$ | 2.31e5$ | 2.31e5$ |
| proposed strategy | 0$ | 0$ | 0$ | 0$ |

Previous findings assume that Typhoon Maria exhibits fixed features, including its trajectory and meteorological factors. The proposed robust emergency dispatch strategy is designed to address emergency scenarios arising from these rigid typhoon characteristics. However, inherent uncertainties may introduce flexible features, leading to multiple typhoon scenarios. Each scenario could yield a distinct set of emergency scenarios, similar to those generated by Typhoon Maria with fixed parameters, as described in Section 4.1. To test the robustness of the proposed robust emergency dispatch strategy under multiple sets of emergency scenarios, the following uncertainties are introduced:

- The maximal wind speed $v_{\mathrm{max,i}}$ at period $i$ is added with a fluctuation term $\Delta v_{\mathrm{max,i}}$ which follows a Gaussian distribution $\Delta v_{\mathrm{max,i}} \in \mathcal{N}(\mu_{\mathrm{v}}, \sigma_{\mathrm{v}}^2)$.
- The radius of maximum wind speed is also added with a fluctuation term $\Delta R_{\mathrm{max,i}}$ which follows a Gaussian distribution $\Delta v_{\mathrm{max,i}} \in \mathcal{N}(\mu_{\mathrm{r}}, \sigma_{\mathrm{r}}^2)$.

In order to study the influence of wind speed's fluctuation on the robustness, the standard deviations of wind speed fluctuation are set to $\sigma_{\mathrm{v}} = 0.2$ m/s, while the means of wind speed fluctuation increase from 0 m/s to 10 m/s in increments of 1 m/s. The average curtailment costs under different $\mu_{\mathrm{v}}$ are shown in Figure 6a. As can be seen, larger $\mu_{\mathrm{v}}$ would cause larger $v_{\mathrm{max,i}}$, as well as line fault probability $Pr^{\mathrm{c}}(B)_{k,i,q}$, which results in early line disconnection. Initially, the proposed strategy can tolerate a certain degree of early line disconnection. However, when $v_{\mathrm{max,i}}$ increases significantly ($\mu_{\mathrm{v}} = 7$), early line disconnection will result in additional curtailment cost.

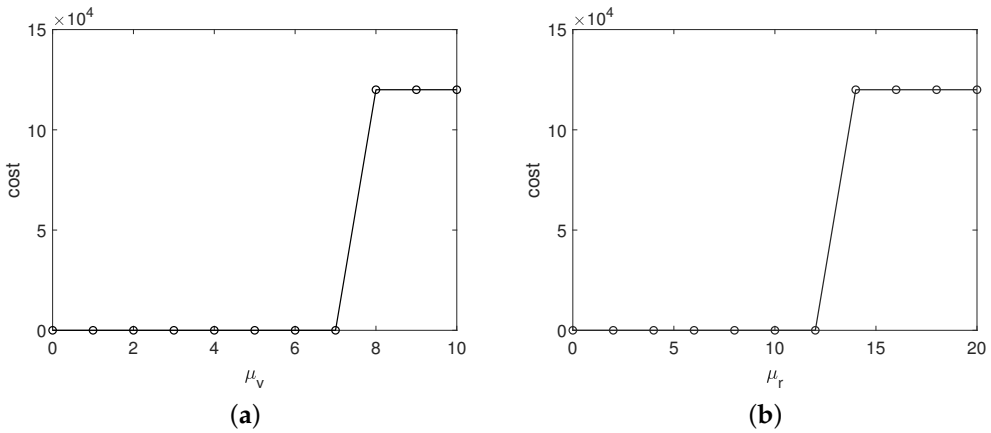


**Figure 6.** Curtailment cost under (**a**) different $\mu_{\mathrm{v}}$ (**b**) different $\mu_{\mathrm{r}}$.

Similarly, the standard deviations of wind speed's fluctuation are set to $\sigma_r = 0.2$ m, while the means of radius fluctuation increase from 0 m to 20 m in increments of 2 m. The average curtailment costs under different $\mu_r$ are shown in Figure 6b. As with Figure 6a, when $v_{max,i}$ increases significantly ($\mu_r = 17$), the short distance between the wind circle and the line leads to increased wind speed and fault probability; consequently, early line disconnection may result in additional curtailment cost.

## 5. Conclusions and Future Work

By studying the time-varying line fault probabilities under typhoons, we develop a robust emergency dispatch strategy considering the spatiotemporal evolution of grid failures. The following conclusions can be achieved based on the case study results:

- Different lines encounter different levels of fatigue damage under the passage of typhoons, causing time-varying fault probabilities of lines and dynamic spatiotemporal evolution of grid failures. The threshold-based method can quickly screen out the irrelevant or less severe scenarios, thus reducing the size of emergency scenarios and complexity of the emergency dispatch model.
- Compared with the non-robust emergency dispatch strategy, the proposed robust emergency dispatch strategy can guarantee the secure operation of power systems under all emergency scenarios of the scenario set without incurring extra load and wind power curtailment costs.

In the future study, the influences of other types of climate disasters will be considered, and the corresponding spatiotemporal revolution of grid failures will be studied. Also, a reduction in the size of the emergency scenario set will be further investigated by achieving the trade-off between computational efficiency elevation and robustness. Optimal line reinforcement, line rerouting and other emergency planning measures under different climate disasters will also be investigated.

**Author Contributions:** Conceptualization, B.R. and D.W.; methodology, B.R. and C.W.; software, B.R. and D.W.; validation, Q.L.; formal analysis, Y.H.; investigation, Y.J. All authors have read and agreed to the published version of the manuscript.

**Funding:** This research was funded by the Science and Technology Project of State Grid Jiangsu Electric Power Company under Grant J2024021 "Research on System Fault Evolution and Risk Assessment Technology Considering Source-Grid Spatio-Temporal Coupling under Extreme Weather Conditions".

**Institutional Review Board Statement:** Not applicable.

**Informed Consent Statement:** Not applicable.

**Data Availability Statement:** Data can be accessed from case studies.

**Conflicts of Interest:** Authors Bixing Ren, Dajiang Wang, Chenggen Wang, Qiang Li, Yingjie Hu, and Yongyong Jia were employed by the company State Grid Jiangsu Electric Power Company Ltd. All authors declare that the research was conducted in the absence of any commercial or financial relationships that could be construed as a potential conflict of interest.

## References

1. Muhtadi, A.; Pandit, D.; Nguyen, N.; Mitra, J. Distributed energy resources based microgrid: Review of architecture, control, and reliability. *IEEE Trans. Ind. Appl.* **2021**, *57*, 2223–2235. [CrossRef]
2. Langeroudi, A.S.G.; Sedaghat, M.; Pirpoor, S.; Fotouhi, R.; Ghasemi, M.A. Risk-based optimal operation of power, heat and hydrogen-based microgrid considering a plug-in electric vehicle. *Int. J. Hydrogen Energy* **2021**, *46*, 30031–30047. [CrossRef]
3. Guo, C.; Ye, C.; Ding, Y.; Wang, P. A multi-state model for transmission system resilience enhancement against short-circuit faults caused by extreme weather events. *IEEE Trans. Power Deliv.* **2020**, *36*, 2374–2385. [CrossRef]
4. Montoya-Rincon, J.P.; Mejia-Manrique, S.A.; Azad, S.; Ghandehari, M.; Harmsen, E.W.; Khanbilvardi, R.; Gonzalez-Cruz, J.E. A socio-technical approach for the assessment of critical infrastructure system vulnerability in extreme weather events. *Nat. Energy* **2023**, *8*, 1002–1012. [CrossRef]
5. Chen, C.; Chen, Y.; Zhao, J.; Zhang, K.; Ni, M.; Ren, B. Data-driven resilient automatic generation control against false data injection attacks. *IEEE Trans. Ind. Inform.* **2021**, *17*, 8092–8101. [CrossRef]

6. Chen, C.; Wang, Y.; Cui, M.; Zhao, J.; Bi, W.; Chen, Y.; Zhang, X. Data-driven detection of stealthy false data injection attack against power system state estimation. *IEEE Trans. Ind. Inform.* **2022**, *18*, 8467–8476. [CrossRef]
7. Zhang, M.; Cai, S.; Xie, Y.; Zhou, B.; Zheng, W.; Wu, Q.; Wen, J. Supply Resilience Constrained Scheduling of MEGs for Distribution System Restoration: A Stochastic Model and FW-PH Algorithm. *IEEE Trans. Smart Grid* **2024**. [CrossRef]
8. Godse, R.; Bhat, S. Mathematical morphology-based feature-extraction technique for detection and classification of faults on power transmission line. *IEEE Access* **2020**, *8*, 38459–38471. [CrossRef]
9. Jaimes, M.A.; García-Soto, A.D.; Martín del Campo, J.O.; Pozos-Estrada, A. Probabilistic risk assessment on wind turbine towers subjected to cyclone-induced wind loads. *Wind. Energy* **2020**, *23*, 528–546. [CrossRef]
10. Mishra, S.; Anderson, K.; Miller, B.; Boyer, K.; Warren, A. Microgrid resilience: A holistic approach for assessing threats, identifying vulnerabilities, and designing corresponding mitigation strategies. *Appl. Energy* **2020**, *264*, 114726. [CrossRef]
11. Younesi, A.; Shayeghi, H.; Safari, A.; Siano, P. Assessing the resilience of multi microgrid based widespread power systems against natural disasters using Monte Carlo Simulation. *Energy* **2020**, *207*, 118220. [CrossRef]
12. Ti, B.; Li, G.; Zhou, M.; Wang, J. Resilience assessment and improvement for cyber-physical power systems under typhoon disasters. *IEEE Trans. Smart Grid* **2021**, *13*, 783–794. [CrossRef]
13. Espinoza, S.; Poulos, A.; Rudnick, H.; de la Llera, J.C.; Panteli, M.; Mancarella, P. Risk and resilience assessment with component criticality ranking of electric power systems subject to earthquakes. *IEEE Syst. J.* **2020**, *14*, 2837–2848. [CrossRef]
14. Bi, W.; Tian, L.; Li, C.; Ma, Z.; Pan, H. Wind-induced failure analysis of a transmission tower-line system with long-term measured data and orientation effect. *Reliab. Eng. Syst. Saf.* **2023**, *229*, 108875. [CrossRef]
15. Fu, B.; Zhao, J.; Li, B.; Yao, J.; Teifouet, A.R.M.; Sun, L.; Wang, Z. Fatigue reliability analysis of wind turbine tower under random wind load. *Struct. Saf.* **2020**, *87*, 101982. [CrossRef]
16. Ceferino, L.; Lin, N.; Xi, D. Bayesian updating of solar panel fragility curves and implications of higher panel strength for solar generation resilience. *Reliab. Eng. Syst. Saf.* **2023**, *229*, 108896. [CrossRef]
17. Chen, L.; Liu, L.; Peng, Y.; Chen, W.; Huang, H.; Wu, T.; Xu, X. Distribution network operational risk assessment and early warning considering multi-risk factors. *IET Gener. Transm. Distrib.* **2020**, *14*, 3139–3149. [CrossRef]
18. Yuan, H.; Xu, Y. Preventive-corrective coordinated transient stability dispatch of power systems with uncertain wind power. *IEEE Trans. Power Syst.* **2020**, *35*, 3616–3626. [CrossRef]
19. Zhou, B.; Wu, J.; Zang, T.; Cai, Y.; Sun, B.; Qiu, Y. Emergency Dispatch Approach for Power Systems with Hybrid Energy Considering Thermal Power Unit Ramping. *Energies* **2023**, *16*, 4213. [CrossRef]
20. Chen, B.; Ye, Z.; Chen, C.; Wang, J.; Ding, T.; Bie, Z. Toward a synthetic model for distribution system restoration and crew dispatch. *IEEE Trans. Power Syst.* **2018**, *34*, 2228–2239. [CrossRef]
21. Qin, Z.; Chen, X.; Hou, Y.; Liu, H.; Yang, Y. Coordination of preventive, emergency and restorative dispatch in extreme weather events. *IEEE Trans. Power Syst.* **2021**, *37*, 2624–2638. [CrossRef]
22. Rong, J.; Zhou, M.; Zhang, Z.; Li, G. Coordination of preventive and emergency dispatch in renewable energy integrated power systems under extreme weather. *IET Renew. Power Gener.* **2024**, *18*, 1164–1176.
23. Huang, L.; Lai, C.S.; Zhao, Z.; Yang, G.; Zhong, B.; Lai, L.L. Robust *Nk* Security-constrained Optimal Power Flow Incorporating Preventive and Corrective Generation Dispatch to Improve Power System Reliability. *CSEE J. Power Energy Syst.* **2022**, *9*, 351–364.
24. Wang, Q.; Yu, Z.; Ye, R.; Lin, Z.; Tang, Y. An ordered curtailment strategy for offshore wind power under extreme weather conditions considering the resilience of the grid. *IEEE Access* **2019**, *7*, 54824–54833. [CrossRef]
25. Zhang, H.; Zhang, S.; Cheng, H.; Li, Z.; Gu, Q.; Tian, X. Boosting the power grid resilience under typhoon disasters by coordinated scheduling of wind energy and conventional generators. *Renew. Energy* **2022**, *200*, 303–319. [CrossRef]
26. Cai, S.; Xie, Y.; Zhang, M.; Jin, X.; Wu, Q.; Guo, J. A Stochastic Sequential Service Restoration Model for Distribution Systems Considering Microgrid Interconnection. *IEEE Trans. Smart Grid* **2023**, *15*, 2396–2409. [CrossRef]
27. Yao, K.; Yu, J.; Xu, T.; Liu, Q. A method to generate dynamic accident set for power grid clustered faults caused by tropical cyclone. *Power Syst. Technol.* **2014**, *38*, 1593–1599.